Biochemical Engineering Journal 205 (2024) 109260

Contents lists available at ScienceDirect

Biochemical Engineering Journal

journal homepage: www.elsevier.com/locate/bej

Regular article

A paradigm shift for biocatalytic microreactors: Decoupling application from reactor design

Marijan Bajić [a], Sansanee Khiawjan [a], Stephen T. Hilton [b], Gary J. Lye [a], Marco P.C. Marques [a,*], Nicolas Szita [a,*]

[a] Department of Biochemical Engineering, University College London, London WC1E 6BT, UK
[b] UCL School of Pharmacy, University College London, London WC1N 1AX, UK

ARTICLE INFO

Keywords:
Microreactors
Residence time distribution
Flow biocatalysis
Enzyme immobilization
Enzymes
Whole cells
Standardisation

ABSTRACT

Microreactors have been successfully applied to execute a broad range of biotransformations in flow. However, microreactors have typically been designed with a specific biotransformation or a specific biocatalyst immobilization method in mind, constraining their wider applicability. Furthermore, their design is typically either applicable for whole-cell or for enzyme biocatalysis, but not for both. We present a novel microreactor design which offers cartridge-like insertion of both immobilised enzymes and cells. A T-shaped lid opens and closes the reaction chamber (whilst leaving the rest of the microreactor unchanged), enables the easy insertion of immobilised biocatalysts, and thus allows the user to configure different reactor types. We demonstrated this novel concept showing three different reactor types: a hydrogel microreactor containing entrapped *E. coli* cells overexpressing transketolase (volumetric productivity of $2.23 \pm 0.83\ mmol_{L\text{-}ERY}\ L_{void}^{-1}\ min^{-1}$), a packed-bed microreactor containing commercial beads with immobilised *Candida antarctica* lipase B (volumetric productivity of $317.69 \pm 96.74\ mmol_{BB}\ L_{void}^{-1}\ min^{-1}$), and a micropillar microreactor containing surface-immobilised ω-transaminase (volumetric productivity of $0.08 \pm 0.02\ mmol_{ACP}\ L_{void}^{-1}\ min^{-1}$). The proposed design showed consistency and robustness for 10 consecutive T-shaped lid 'open and close' cycles and withstood the pressure of at least 4 bar. Design analysis further included Computational Fluid Dynamics models and Residence Time Distribution measurements. The presented design offers a standardised approach for multiple applications, underpinning process development and paving the way for off-the-shelf microreactor technology for biocatalysis.

1. Introduction

Performing biocatalysis in flow has received renewed interest in recent years in the wake of the successes in flow chemistry [1,2], and a large number of different continuous-flow microreactors successfully demonstrated a broad range of biocatalytic applications [3,4]. The small dimensions characteristic of these devices can offer advantages for process development compared to traditional set ups. Transport phenomena are often improved, there is good spatiotemporal control over process conditions, and compartmentalisation of the reactions is feasible [5,6]. The latter is of particular interest if complex cascade reactions are envisaged and if distinct reaction conditions are required for products that are difficult to synthesize. Additionally, by implementing side-entries, substrate can be added as the reaction progresses, thereby creating *in situ* substrate supply approaches [7]. Furthermore, microreactors can also be coupled in-line with micro-scale unit operations that facilitate work up to remove and purify product [8–10]. Finally, sensor integration facilitates real-time monitoring of reaction progress [11], and allows implementation of control strategies [12]. With all the advances made, standardised microreactor designs would appear to be the next logical step forward for the field. Standardised approaches could yield universal platforms and thus ultimately enhance industrial uptake.

Biocatalytic reactions use either isolated enzymes or whole cells [6], and both isolated enzymes and whole cells can be used either in solution or in immobilised form. The latter option is preferable when biocatalyst reuse, stability, and long-term operation are desired [13], and generally provides greater flexibility in reactor operation. Biocatalytic microreactors have been successfully demonstrated with both enzymes and cells as biocatalysts, and many immobilization methods have been implemented. However, immobilization method and microreactor design are not typically independent from each other. *Ex situ* immobilization methods, such as biocatalysts attached to particles for subsequent insertion into a microreactor [14–16], or *in situ* immobilization

* Corresponding authors.
E-mail addresses: marco.marques@ucl.ac.uk (M.P.C. Marques), n.szita@ucl.ac.uk (N. Szita).

https://doi.org/10.1016/j.bej.2024.109260
Received 13 October 2023; Received in revised form 2 February 2024; Accepted 11 February 2024
Available online 14 February 2024

Legend

Latin symbols

BPN	biocatalyst productivity number [$mmol_{product}\ mg^{-1}_{biocatalyst}$; $mmol_{product}\ g^{-1}_{biocatalyst}$].
c	concentration of substrate/product [mM].
c_B	concentration of biocatalyst [$mg_{biocatalyst}\ mL^{-1}_{void}$; $mg_{biocatalyst}\ L^{-1}_{void}$].
D	diffusion coefficient [$m\ s^{-2}$].
d	depth of the reaction chamber [µm, m].
d_{N435}	mean diameter of N435 [µm].
E_{cal}	computed E curve.
E_{exp}	experimental E curve.
F_{cal}	computed F curve.
l	length of the reaction chamber [mm, m].
M	units of tracer injected into the system [mmol].
m	mass [µg, mg].
n	sample size [–].
Q_P	volumetric productivity [$mmol_{product}\ L^{-1}_{void}\ min^{-1}$].
Q_V	volumetric flow rate [$µL\ min^{-1}$; $L\ min^{-1}$].
Re	Reynolds number [–].
s	skewness [–].
SA_B	specific activity of biocatalyst [$U\ mg^{-1}_{biocatalyst}$].
T	temperature [°C].
t	time [s, min].
u	fluid velocity magnitude [$mm\ s^{-1}$; $m\ s^{-1}$].
V	volume of the reaction chamber [µL; mL].
V_V	void volume of the reaction chamber [µL].
w	width of the reaction chamber [mm, m].
X	fractional conversion [%].

Greek symbols

α	level of significance [–].
Υ_B	biocatalyst load [$U\ mL^{-1}_{void}$].
ε_{RC}	porosity of the reaction chamber [—].
$\sigma(t)^2$	variance [min^2].
$\sigma(\theta)^2$	dimensionless variance [–].
τ	mean residence time [min].
τ_{RC}	mean residence time in the reaction chamber [min].

Abbreviations and acronyms

ACE	acetaldehyde.
ACP	acetophenone.
APTES	(3-aminopropyl)triethoxysilane.
BB	butyl butyrate.
CaLB	*Candida antarctica* lipase B.
CFD	computational fluid dynamics.
DCW	dry cell weight.
GA	glycolaldehyde.
GC	gas chromatography.
GTA	glutaraldehyde.
HPA	lithium-β-hydroxypyruvate.
HPLC	high-performance liquid chromatography.
ID	inner diameter.
N435	Novozym® 435.
OD	outer diameter.
$OD_{600\ nm}$	optical density at 600 nm.
PDMS	polydimethylsiloxane.
PEEK	polyether ether ketone.
PFA	perfluoroalkoxy.
PLP	pyridoxal 5′-phosphate.
PYR	sodium pyruvate.
RTD	residence time distribution.
TFA	trifluoroacetic acid.
ThDP	thiamine diphosphate.
TK	transketolase.
VB	vinyl butyrate.
L-ALA	L-alanine.
L-ERY	L-erythrulose.
L-TRY	L-tryptophan.
ω-TAm	ω-transaminase.
(S)-α-MBA	(S)-(-)-α-methylbenzylamine.
1-BUT	1-butanol.

methods, for example with biocatalysts attached to the surface of the inner channel walls [17,18], or to nanostructures [19,20], or with biocatalysts entrapped into hydrogel sheets [21], are implemented with different microreactor designs. Furthermore, implementing *in situ* immobilization methods can constrain repeated use of the microreactor, which in turn drive cost and increase environmental footprint. Therefore, as a first step towards standardised designs for biocatalytic microreactors, it is necessary to de-couple design from immobilization method, such that one device design can sustain a broad range of different immobilization methods.

Microreactors, particularly when fabricated as microfluidic channels or when made from capillaries, are enclosed devices. Owing to their small sizes, it is non-trivial to include ports with direct access to the reaction chamber (such as known from large stirred tank reactors). Immobilization supports must therefore be flowed in from an upstream fluidic port to the reaction chamber or be generated *in situ*, which limits the type of immobilization supports that can be loaded into a microreactor. Establishing a versatile microreactor capable of accommodating a diverse range of immobilization methods therefore requires a novel design with simple, cartridge-like insertion of immobilised enzymes or cells into the flow-channel. We have previously solved a similar challenge for microfluidic cell culture devices. Reichen et al. developed a modular microfluidic cell culture device with a re-sealable culture chamber [22,23]. A 'T-shaped' lid in this design allowed opening and closing of the culture chamber alone, i.e. leaving the other microfluidic device structures enclosed. With this design, we successfully loaded a broad range of different materials: gels for the attachment of cells, suspended cell solutions, sub-millimetre sized cell clusters, and three-dimensional embryoid bodies [24–26]. The device was applied across many process-related applications in regenerative medicine, demonstrating the versatility of the design [24–29].

In this article, we hypothesised that the previously introduced design with a T-shaped lid [22] is applicable to biocatalysis, that the design would facilitate integration of different immobilization supports, and therefore provide a standardised framework for performing biocatalysis on a microreactor scale. To test this hypothesis, we adapted the design and operated the modified device as three different microreactor types based on the immobilization carriers used: (i) a hydrogel microreactor containing entrapped *E. coli* cells overexpressing transketolase (TK; EC 2.2.1.1), (ii) a packed-bed microreactor containing adsorbed *Candida antarctica* lipase B (CaLB; EC 3.1.1.3), and (iii) a micropillar microreactor containing covalently immobilised ω-transaminase (ω-TAm; EC 2.6.1.18). These enzyme systems represent key industrial biotransformation for the synthesis of APIs and synthons [30–32]. For each microreactor type we performed the Residence Time Distribution (RTD) analysis, which is an effective method to characterise microreactor

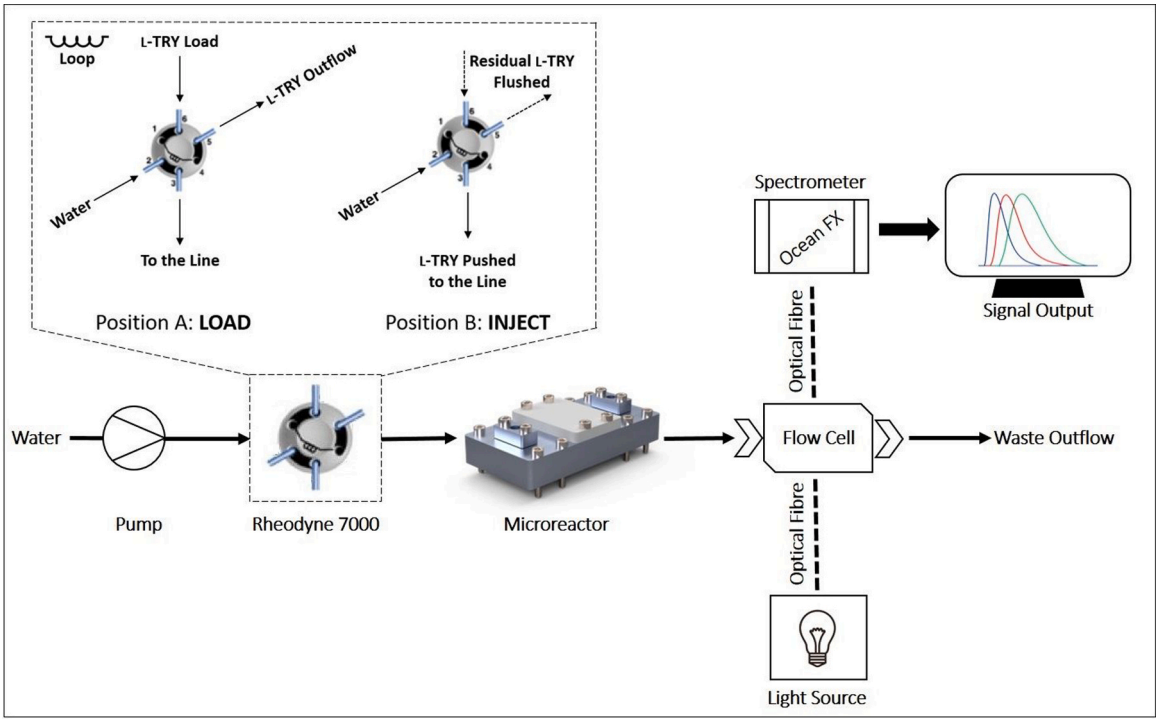

Fig. 1. Schematic of the setup for the RTD analysis performed by a stimulus-response experiment with pulse input of L-TRY. The Rheodyne 7000 valve flow path diagrams for load position (A) and for injection position (B) are shown in the inset picture. The estimated total volume of tubing leading up to the flow cell was ≈110 μL, and it was presumed to have a negligible overall impact on the experimental $c_{L\text{-}TRY}(t)$ distribution.

performance [15,33–35]. Finally, Computational Fluid Dynamics (CFD) models were developed to evaluate the hydrodynamics in this novel microreactor.

2. Materials and methods

2.1. Chemicals

Unless otherwise stated, all chemicals and reagents were purchased from Sigma-Aldrich (Gillingham, UK) and were of analytical grade. Ultrapure water (resistivity of 18.2 MΩ × cm) obtained from a Milli-Q® purification system (MilliporeSigma, Burlington, MA, USA) was used in all experiments.

2.2. Microreactor design and fabrication

All components of the device and moulds were designed using Solidworks® 2021 (Dassault Systèmes, Vélizy-Villacoublay, France). Two rigid aluminium (Al) plates formed a compressible seal over a microfluidic chip (compression factor up to 10%), which contained the fluidic channels and a reaction chamber. The Al parts were fabricated by CNC machining (TM-1 P CNC Toolroom Mill, Haas Automation, Norwich, UK) while the poly(methyl methacrylate) (PMMA; RS Pro, Corby, UK) part was cut to size using a CO_2 laser marking head (Epilog Laser, Clevedon, UK). The microfluidic chip was fabricated from polydimethylsiloxane (PDMS; SYLGARD™ 184 Silicone Elastomer Kit, Dow Corning, Midland, TX, USA) according to the protocol outlined elsewhere [23,25]. The moulds and the T-shaped lid were 3D-printed on a Form 3+ printer using the proprietary resins Rigid 4000 and Clear, respectively (Formlabs Inc., Somerville, MA, USA). The 3D prints were printed at a resolution of 50 μm, followed by thorough washing with an excessive amount of isopropyl alcohol (IPA; RS Pro) for 15 min and cured under ambient conditions, i.e., no UV curing was applied.

2.3. Computational Fluid Dynamics models

3D CFD models were developed to compute fluid velocity profiles and mass transfer of the tracer used in the RTD analysis (see Section 2.4). The *Laminar Flow* and *Transport of Diluted Species* interfaces of Comsol Multiphysics® 5.3 (Comsol, Inc., Stockholm, Sweden) were applied to create the models.

The governing Navier-Stokes and continuity equations were solved for pure water at 20 °C as the working fluid, and the flow was considered laminar, incompressible, isothermal, and at steady-state. The boundary conditions were set as follows: at the microreactor inlet to an average velocity calculated from the applied inlet volumetric flow rates (Q_V = 300 μL min^{-1} to 1000 μL min^{-1}), at the microreactor outlet to zero pressure, and at the walls no-slip [22]. Velocity profiles and corresponding Reynolds numbers (*Re*) were obtained for all microreactor types.

Following the fluid flow velocity profiles, non-stationary models were developed to simulate the mass transfer of the tracer injected in a fully-developed flow (Section 2.4), considering convective transport (axial direction) and diffusion (radial and axial direction). The diffusion coefficient of the tracer ($D_{L\text{-}TRY} = 8.54 \times 10^{-10}$ m^2 s^{-1}) was approximated by the Wilke-Chang correlation [36]. The models considered 1 mM tracer concentration at the microreactor inlet and a concentration distribution at the microreactor outlet. The *F* curve (F_{cal}) obtained from the computed concentration profile at the microreactor outlet was then used to get the calculated *E* curve (E_{cal}), following that $E_{cal} = dF_{cal}/dt$.

In all models, tetrahedral meshing elements were set to *finer*, resulting in a total of around 5 million elements in the physical domains of the microreactors. To reduce computational time when running simulations in the packed-bed microreactor, the spherical beads were substituted by cylindrical micropillars with base diameters matching the distribution of the spherical beads. A Python script was developed to randomize spatial positions of the cylindrical micropillars while matching the desired bed porosity.

2.4. Residence Time Distribution analysis

The RTD was determined experimentally using the pulse input technique using L-tryptophan (L-TRY; Serva Electrophoresis, Heidelberg, Germany) as a non-reactive tracer. The set up (Fig. 1) was comprised of a Nemesys syringe pump (Cetoni, Korbussen, Germany), connected to a Valvemate® actuator equipped with a Rheodyne 7000 switching valve (Gilson, Middleton, WI, USA). The valve actuator was connected to the microreactor, and this was connected subsequently to a flow cell (FIA-Z-SMA-PEEK, Ocean Insight, Orlando, USA). The read-out from flow cell was performed through two optical fibres that were connected to the Ocean FX spectrometer and the light source DH-2000-BAL (both from Ocean Insight). Connections between the different parts of the set up were made out of perfluoroalkoxy (PFA) tubing (1.59 mm OD × 0.75 mm ID; Vici AG International, Schenkon, Switzerland).

Different flow rates were tested, ranging from 300 μL min^{-1} to 1000 μL min^{-1}. The valve actuator injected a pulse of 1 mM L-TRY, corresponding to a slug of 7.5 μL (≈1.53 $\mu g_{L\text{-}TRY}$). L-TRY was continuously measured at the microreactor outlet at 280 nm and 10 Hz. The pulse-response curves were obtained by averaging every ten measurements [15], allowing to obtain the experimental E curve, E_{exp} [min^{-1}] ((1)), mean residence time, τ [min] ((2)), variance, $\sigma(t)^2$ [min^2] ((3)), dimensionless variance, $\sigma(\theta)^2$ [–] ((4)), and skewness, s [–] of the $c_{L\text{-}TRY}(t)$ distribution ((5));

$$E = \frac{C_{L-TRY}}{M_{L-TRY}/Q_V} \quad (1)$$

$$\tau = \frac{\sum tC_{L-TRY}}{\sum C_{L-TRY}} \quad (2)$$

$$\sigma(t)^2 = \frac{\sum (t)^2 C_{L\text{-}TRY}}{\sum C_{L\text{-}TRY}} \tau^2 \quad (3)$$

$$\sigma(\theta)^2 = \frac{\sigma(t)^2}{\tau^2} \quad (4)$$

$$S = \frac{\sum (t=\tau)^3 C_{L\text{-}TRY}}{\sigma^3 \sum C_{L\text{-}TRY}} \quad (5)$$

where, $c_{L\text{-}TRY}$, $M_{L\text{-}TRY}$, t and Q_V represent concentration of tracer [mM], units of tracer injected into the system [mmol], time [min], and volumetric flow rate [L min^{-1}], respectively. We assumed an isothermal homogeneous system with a fully-developed steady-state flow at the time of tracer injection and an inert tracer that does not disturb the flow.

2.5. Biocatalysts preparation and enzyme activity

2.5.1. E. coli cells overexpressing transketolase

E. coli XL10-Gold with plasmid pQR791 (wild-type TK) was prepared in-house according to the protocol described elsewhere [7]. The TK specific activity in *E. coli* cells ($SA_{E.\ coli}$) was determined using a 50 mM equimolar solution of lithium β-hydroxypyruvate (HPA) and glycolaldehyde (GA) containing 2.4 mM thiamine diphosphate (ThDP) and 9.8 mM $CaCl_2$ in HEPES buffer (50 mM; pH 7.0). To this, 0.43 mg of dry cell weight (DCW) per mL was added. The reaction mixture was continuously stirred at 300 rpm and 20 °C. At predetermined times, 50 μL aliquots were taken, mixed with 450 μL 0.1% v/v trifluoroacetic acid (TFA) solution, and analysed by HPLC (Section 2.8.3).

2.5.2. Candida antarctica lipase B

The activity of Novozym® 435 (N435) was determined using a 600 mM equimolar solution of vinyl butyrate (VB) and 1-butanol (1-BUT) in *n*-heptane to which 5 mg_{N435} mL^{-1} was added. The reaction mixture was continuously stirred at 700 rpm and 20 °C. At predetermined times, 180 μL aliquots were taken and analysed by GC (Section 2.8.4). The specific activity of CaLB was expressed per mass of N435, SA_{N435} [U mg^{-1}_{N435}] or per mass of CaLB, SA_{CaLB} [U mg^{-1}_{CaLB}], where U is defined as the amount of N435 or CaLB that catalyse the formation of 1 μmol of the product per minute under the specified experimental conditions.

2.5.3. ω-Transaminase

ω-TAm lysate was obtained using *E. coli* BL21-Gold (DE3) strain containing plasmid pQR801, according to the previously described protocols [37]. The specific activity ω-TAm lysates ($SA_{\omega\text{-}TAm\ lysate}$) was determined using a 20 mM equimolar solution of (*S*)-(-)-α-methylbenzylamine ((*S*)-α-MBA) and sodium pyruvate (PYR; Alfa Aesar, Heysham, UK), containing 1 mM pyridoxal 5′-phosphate (PLP), in HEPES buffer (50 mM; pH 7.5). To this, 0.47 ± 0.11 mg mL^{-1} of total protein was added. The reaction mixture was continuously stirred at 300 rpm and 20 °C. At predetermined times, 50 μL aliquots were taken, mixed with 450 μL of a 0.1% v/v TFA solution, and analysed by HPLC (Section 2.8.3). The $SA_{\omega\text{-}TAm\ lysate}$ was expressed per mass of the total protein [U $mg^{-1}_{total\ protein}$], where U is defined as the amount of total protein that catalyse formation of 1 μmol of the product per minute under the specified experimental conditions.

2.6. Immobilization methods

2.6.1. Entrapment of E. coli cells

E. coli cells were re-suspended in HEPES buffer (50 mM; pH 7.0) and mixed with an alginate (CAS No.: 9005–38–3; Product No.: W201502) stock solution to a final concentration of 2.15 ± 0.10 mg_{DCW} mL^{-1} and alginate concentration of 2.5% w/v. 350 μL of this mixture was spread into the 3D mould's each inner well (Fig. S1, Appendix A) to ensure complete filling. To initiate gelation, a solution of 2.5% w/v $CaCl_2$ was sprayed over the mixture at a distance of 30 cm above the wells. After 2 min, the mould was completely filled with cross-linking solution, covering the alginate hydrogel entirely and left for 1 h at 20 °C. The final alginate hydrogel sheet was peeled off and rinsed with HEPES buffer (50 mM; pH 7.0) before use.

2.6.2. Covalent immobilization of ω-transaminase

The 3D-printed T-shaped lid was treated with 95% H_2SO_4 (VWR International, Lutterworth, UK) for 5 min and then rinsed with water. Afterwards, the entire lid was placed in a 10% v/v solution of (3-aminopropyl)triethoxysilane (APTES) for 18 h at 20 °C. Following another rinsing step with water, the entire lid was placed in a 10% v/v solution of glutaraldehyde (GTA) for 4 h at 20 °C. After a final rinse with water, the lid was inserted into the microreactor and a 30% v/v solution of ω-TAm lysate (9.4 ± 2.2 $mg_{total\ protein}$ mL^{-1}) was circulated through the microreactor at a flow rate of 2 μL min^{-1} for 18 h at 20 °C. The microreactor was flushed with HEPES buffer (50 mM; pH 7.5) containing 1 mM PLP at a flow rate of 1 mL min^{-1} (×10 the volume of the reaction chamber) before use. Immobilization efficiency was calculated according to adapted protocol (Fig. S2, Appendix A).

2.7. Continuous biocatalytic reaction in microreactor

2.7.1. Peripheral connections

The microreactor was connected to a gastight glass syringe (#1005, #1010, or #1025; Hamilton Company, Reno, NV, USA) using PFA tubing (1.59 mm OD × 0.75 mm ID) with polyether ether ketone (PEEK) female-to-female Luer adapters and flangeless fittings (Vici AG International). The continuous flow was provided using the Nemesys syringe pump.

2.7.2. Transketolase-catalysed reaction (whole cells)

Alginate sheets containing the *E. coli* cells overexpressing TK (Section 2.6.1) was carefully fixed to the bottom of a tailored T-shape lid by means of a double-sided adhesive tape (ARcare® 90445, thickness

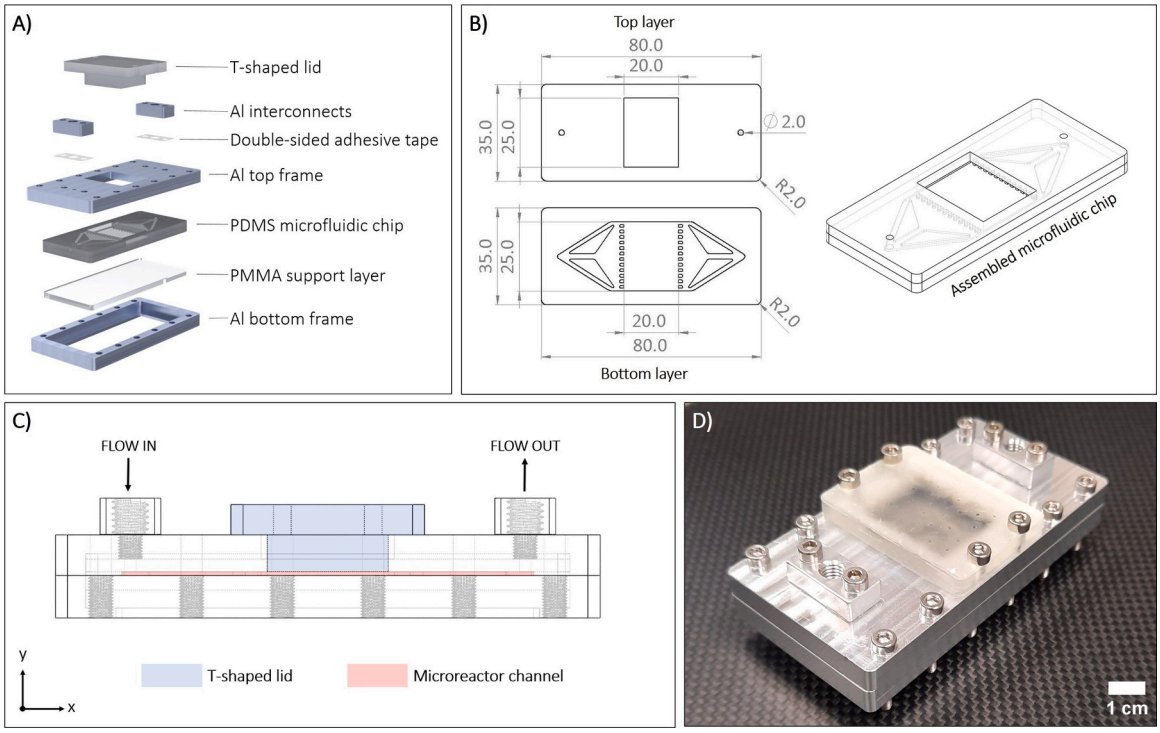

Fig. 2. The key elements of the microreactor. **A)** Exploded view showcasing the main assembly components. **B)** Design specifications of the PDMS microfluidic chip, with characteristic dimensions provided in millimetres. **C)** Cross-sectional view of the microreactor, highlighting the alignment of key assembly components. **D)** Image of the fully assembled microreactor.

without liners ≈81 μm [38]; Adhesives Research, Limerick, Ireland). A 60 mM equimolar solution of HPA and GA containing 2.4 mM ThDP and 9.8 mM $CaCl_2$ in HEPES buffer (50 mM; pH 7.0), was continuously pumped at flow rates set between 10 μL min^{-1} and 149 μL min^{-1}. At predetermined times, 50 μL aliquots were collected at the microreactor outlet and mixed with 450 μL of a 0.1% v/v TFA solution. Samples were analysed by HPLC (Section 2.8.3).

2.7.3. Lipase-catalysed reaction

N435 beads were sieved through a system of two Fisherbrand™ stainless steel sieves with woven wire mesh with pore sizes of 710 μm and 500 μm (Thermo Fisher Scientific, Waltham, MA, USA). Bead diameters were measured using ImageJ (National Institutes of Health, Bethesda, USA) using a light microscope equipped with a photo camera (Nikon Eclipse Ti, Tokyo, Japan). Bead mean diameter (d_{N435} = 608 ± 78 μm) and diameter size distribution were determined from n = 100 (Fig. S3, Appendix A).

N435 beads were manually loaded onto double-sided adhesive tape pre-attached to the bottom of the T-shaped lid and gently pressed down using a stainless steel spatula, as previously described [15]. The excess amount was carefully removed using soft brush, and weight, leaving behind a bed of N435 beads (m_{N435} = 67.9 ± 3.4 mg; m_{CaLB} = 6.79 ± 0.34 mg). The T-shaped lid was then inserted to create the packed-bed microreactor. A 230 mM equimolar solution of VB and 1-BUT in n-heptane was continuously pumped at flow rates set between 87 μL min^{-1} to 1750 μL min^{-1}. At predetermined times, 180 μL aliquots were collected at the microreactor outlet and analysed by GC (Section 2.8.4).

2.7.4. Transaminase-catalysed reaction

Upon successful insertion of the T-shape lid containing immobilised ω-TAm (Section 2.6.2), a 10 mM equimolar solution of (*S*)-α-MBA and PYR containing 1 mM PLP in HEPES buffer (50 mM; pH 7.5) was then continuously pumped at flow rates set between 6 μL min^{-1} and 134 μL min^{-1}. At predetermined times, 50 μL aliquots were collected at the microreactor outlet, and mixed with 450 μL of a 0.1% v/v TFA solution. Samples were analysed by HPLC (Section 2.8.3).

2.8. Analytical methods

2.8.1. E. coli dry cell weight

E. coli suspensions with known OD_{600} values were prepared and subjected to centrifugation at 3274 × g_{force} for 5 min at 4 °C (Centrifuge 5910 R; Eppendorf, Hamburg, Germany). Supernatant was discarded and the cell pellets were dried at 60 ℃ (UFP400, Memmert GmbH, Schwabach, Germany) until a constant weight was measured (Fig. S4, Appendix A).

2.8.2. Protein quantification

Bradford reagent (Thermo Fisher Scientific) was used for total protein concentration quantification with bovine serum albumin (BSA) as standard [39]. All samples were measured on a CLARIOstar Plus microplate reader (BMG Labtech, Aylesbury, UK).

2.8.3. Reagent analysis by HPLC

HPLC analysis was performed on a Dionex UltiMate 3000 system (Thermo Fisher Scientific). Prior to analysis, all samples were centrifuged at 12,298 × g_{force} for 5 min, and 4 °C (Centrifuge 5424 R; Eppendorf). HPA and L-ERY were analysed on an Aminex HPX-87 H column (300 mm × 7.8 mm; Bio-Rad, Hemel Hempstead, UK) with a 0.6 mL min^{-1} isocratic elution of 0.1% v/v TFA at 60°C and detection at 210 nm. (*S*)-α-MBA and ACP were analysed on an ACE 5 C18 RP column (150 mm×4.6 mm, 5 μm particle size; Advanced Chromatography Technologies, Aberdeen, UK) with detection at 254 nm. The mobile phase consisted of 0.1% v/v TFA at a flow rate of 1 mL min^{-1}, with a gradient of acetonitrile (Thermo Fisher Scientific) from 15% to 72% over 9 min, followed by a 2-min equilibration period [37].

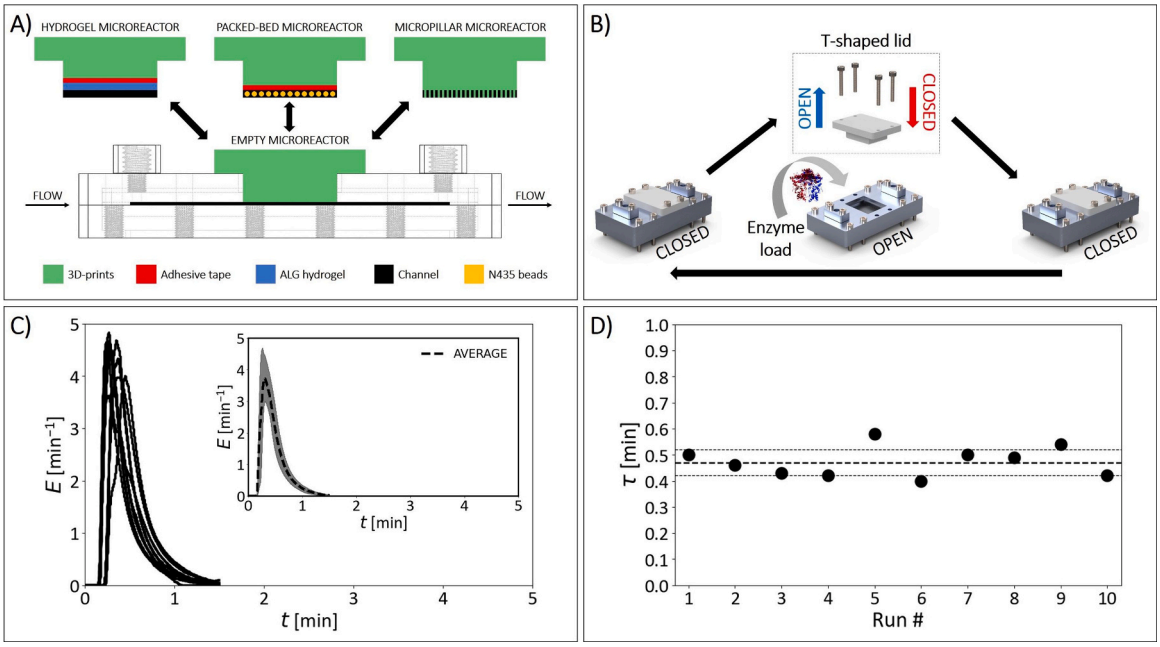

Fig. 3. Key aspects of the T-shaped lid design and operation. **A)** Versatile microreactor configurations enabled by the lid design. **B)** Visual representation of the lid replacement process. **C)** Experimental *E* curves derived from the RTD measurements for 10 consecutive lid replacements. The inset graph shows the average value and standard deviation. **D)** Mean residence times calculated from the experimental *E* curves. The dashed lines indicate the average value and standard deviation (τ = 0.47 ± 0.05 min).

2.8.4. Reagent analysis by GC

VB and BB were analysed using a TRACE™ 1300 gas chromatograph (Thermo Fisher Scientific) equipped with a flame ionization detector and a fused silica capillary column (Rxi™ 5Sil MS, 0.25 mm ID; Restek Corporation, Bellefonte, PA, USA). Hydrogen (35 mL min^{-1}) and air (350 mL min^{-1}) were used to make up the carrier gas. The oven temperature was initially set to 100 °C at the time of injection, after which it was held constant for 1 min. Afterwards, the temperature was increased to 200 °C at a rate of 35 °C min^{-1}, and it was kept constant until the end of the run (5 min).

2.8.5. Evaluation of microreactor biocatalytic efficiency

The biocatalytic efficiency of the microreactors was determined using the concentration of at least one substrate and one product in the outflow, by calculating the fractional conversion (X=($c_{substrate\_in}$−$c_{substrate\_out}$)/$c_{substrate\_in}$, [%]), volumetric productivity (Q_P=$c_{product\_out}$/τ_{RC}, [$mmol_{product}$ L_{void}^{-1} min^{-1}]), and biocatalyst productivity number expressed as the amount of product produced per mass of biocatalyst (BPN=$c_{product\_out}$/c_B, [$mmol_{product}$ $mg_{biocatalyst}^{-1}$]) [14,40], where $c_{substrate\_in}$, $c_{substrate\_out}$, $c_{product\_out}$, c_B, and τ_{RC} are the inlet substrate concentration [mM], outlet substrate concentration [mM], outlet product concentration [mM], biocatalyst concentration [$mg_{biocatalyst}$ L_{void}^{-1}], and mean residence time in the reaction chamber [min], respectively.

2.9. Statistical analysis

Except for the specific activity measurements which were done in duplicates, all experiments were done at least in triplicates. Unless otherwise specified, results are presented as mean ± standard deviation. The Chi-squared test (χ^2 test) was used to determine the goodness-of-fit between the RTD experimental results and the theoretical model.

3. Results and discussion

Biocatalytic microreactors have typically been designed with a particular biotransformation or a particular immobilisation method in mind. Our aim was to show that it is possible to design a microreactor which supports a range of different immobilisation methods. Additionally, we wanted a design that allows inserting both enzymes and cells into the microreactor easily. With a microreactor like this, a large number of different biotransformations could then be performed. Furthermore, such a versatile reactor would present a significant step towards greater standardisation in the field.

3.1. Microreactor design

The design of the microreactor closely followed the conceptual approach presented by Reichen et al. [22,23]. The reactor consisted of a T-shaped lid made from 3D-printed resin; two interconnects, and a top and bottom frame made from aluminium (Al); a microfluidic chip made from poly(dimethylsiloxane) (PDMS); and a support layer made from poly(methylmethacrylate) (PMMA) (Fig. 2A).

The top Al frame was designed to house the lid, and contained a recess which positioned the microfluidic chip. Additionally, two interconnects were mounted on the top Al frame, and a double-sided adhesive tape provided the fluidic seal between the frame and interconnects (which accommodated the flangeless fittings). The top frame also contained clearance holes while the bottom frame included threaded holes for M3 screws to clamp the microfluidic chip. The bottom Al frame held the PMMA layer which in turn mechanically supported the microfluidic PDMS chip and allowed visualization of the flow due to its optical transparency. The microfluidic chip was made from two PDMS layers, each 3 mm thick (Fig. 2B). The top PDMS layer comprised two fluidic ports that aligned with the centre bore of the interconnects, and a rectangular opening defining the top part of the reaction chamber. The bottom PDMS layer included the microfluidic channels and the bottom part of the reaction chamber. Similar to the design by Reichen et al. [22,23], three channels which led to the flow equalization (or perfusion) barriers expanded the flow from the fluidic inlet port before the flow entered the reaction chamber. The flow exited the chamber through an identical channel manifold on the other side of the chamber (and through the fluidic outlet port). Different from the design presented by Reichen et al. [22], the chamber measured 20 mm in the direction of flow by 25 mm across the flow and contained only 12 equidistantly

Table 1
Heights of the 'vertical' bar for the different microreactor types and immobilization supports.

Microreactor type	Height of 'vertical' bar [mm]	Chamber dimensions and additional information
Empty / Free enzymes	7.00	No immobilization support required. Height of the chamber was 600 μm.
Hydrogel	6.30	Shortened 'vertical' bar accommodated the adhesive tape (≈80 μm) and hydrogel sheet (≈590 μm), leading to a total height of ≈6.97 mm.
Packed-bed	6.92	The overall height was increased by the thicknesses of both adhesive tape and bead layer, which is represented by the mean bead diameter (≈610 μm), leading to a total height of ≈7.61 mm.
Micropillar	7.00	The overall height was increased by the height of micropillars (≈650 μm), leading to a total height of ≈7.65 mm.

positioned flow equalization barrier on each side of the chamber. The resulting 13 apertures were each 600 μm high and 1 mm wide. Additionally, the chamber itself was not recessed with respect to the flow barriers. Instead, all structures in the bottom part of the reactor had a uniform depth of 600 μm. The chamber was thus enclosed to the bottom by PDMS, by PDMS and the flow barriers to the sides of the chamber in flow direction, and by PDMS to the other two sides.

Finally, the top of the reaction chamber was closed with a T-shaped lid, meaning a lid comprised of an upper 'horizontal' bar and a lower 'vertical' bar. The 'vertical' bar formed a press-fit with the microfluidic PDMS chip (Fig. 2C and Fig. 2D) [22]. The height of the 'vertical' bar determined the depth of the reaction chamber. The 'horizontal' bar contained four bores to attach the lid to the aluminium top frame with M3 screws. When attaching the lid with the screws, the 'horizontal' bar acted as a bed stop when the lower 'vertical' bar was pushed into the opening of the aluminium frame, ensuring reproducible positioning of the 'vertical' bar with respect to the reaction chamber. Thanks to the T-shaped lid, opening and closing of the reaction chamber was straightforward. Importantly, opening and closing of the chamber became completely independent from the assembly of the rest of the microreactor. This meant that the microreactor had two configurations: an 'open' configuration with the lid removed, and a 'closed' configuration with the lid attached.

3.2. Cartridge-like insertion of biocatalysts

In addition to sealing the reaction chamber, and achieving the desired depth of the chamber, we wanted to see whether the lid could act as a conduit to easily introduce biocatalysts into a reaction chamber and, simultaneously, enable insertion of different immobilisation supports. To test this, we 3D printed three different lids and included three different immobilisation supports to them (Fig. 3A). The first lid had a slightly shortened 'vertical' bar (compared to the length of the bar for the empty microreactor chamber) with a double-sided adhesive tape glued to its bottom surface, to which we then attached ALG hydrogel sheets. The second lid also included a double-sided adhesive tape but held N435 beads. The third lid had an array of micropillars at the bottom end of the 'vertical' bar. The micropillars were arranged in a hexagonal pattern and were fabricated to be slightly longer in size than the depth of the chamber. This ensured that the micropillars touched the PDMS layer at the bottom of the chamber. The dimensions for the three different lids are found in Table 1.

Using the lid, we were therefore able to elegantly circumvent the challenge of introducing biocatalysts into a typically 'closed' microreactor (Fig. 3B). With our microreactor design, in the 'open' configuration, the lid is prepared according to the desired combination of immobilisation method and choice of biocatalyst. Additionally, using 3D-printing, the preparation of different lid geometries can be achieved rapidly and with little effort. Furthermore, with the lid separate and outside of the microreactor, the bottom surface of the 'vertical' bar is easily accessible for different immobilisation chemistries. Moreover, removing the lid can also be used to simply refresh the biocatalysts to extend the duration of the continuous biotransformation. Once the biocatalyst immobilisation is completed and the lid is ready, the lid is inserted into the microfluidic PDMS chip, returning the microreactor to its 'close' configuration and thus ready to perform the biotransformation. We demonstrated this for three different immobilisation methods, which led to the following three microreactor types: a hydrogel microreactor, a packed-bed microreactor, and a micropillar microreactor. Therefore, the T-shaped lid does not only facilitate cartridge-like and easy insertion of biocatalysts. At the same time, depending on the chosen modification of the lid, we also effectively created three different reactor types based on one single microreactor design (Fig. 3A and Fig. 3B, Table 1).

We had previously demonstrated that a T-shaped lid can be removed and reinserted into a microfluidic device for up to 30 times [22]. Additionally, for this microreactor, we attained leak-free operation of the microreactor by tightening all M3 screws to a torque of 400 cNm. Nonetheless, we wanted to show that removing and reattaching the lid (with the mentioned torque) would not significantly alter the performance of the device as a microreactor. To do so, we evaluated its performance using RTD analysis. Fig. 3C shows the E curves for ten independent opening/closing cycles of the lid. The experimental E curves maintained their shape and amplitude reasonably well, indicating that the microreactor operated under similar conditions in each of the cycle. A closer analysis of the mean residence times revealed a mean of $\tau = 0.47$ min, with a coefficient of variation of 11% (Fig. 3D), which could be the result of small deformations of the PDMS layers when inserting the lid. Additionally, the robustness of operation and sealing was evaluated by conducting burst pressure measurements after each cycle. The microreactor withstood pressures of at least 4 bars without any visual signs of leakage in each cycle (Fig. S5, Appendix A). It was therefore possible to open and close the lid over 10 times without having to replace the PDMS microfluidic chip.

3.3. Fluid flow velocity profiles of the microreactor types

To establish whether a model understanding of the performance of this novel microreactor concept can be attained, we first developed CFD models to evaluate the fluid flow through the three different microreactor types. For these models, we used the properties of pure water at 20 °C as the working fluid, and the flow was considered laminar, incompressible, isothermal, and at steady-state. The volumetric flow rates of 300 μL min^{-1}, 500 μL min^{-1}, 700 μL min^{-1} and 1000 μL min^{-1} were imposed at the inlet, and a pressure of zero set at the outlet. The models were then subsequently used to calculate theoretical response curves from a tracer pulse experiments (see Section 2.4). Fig. 4 shows the results of these model calculations for a flow rate of 1000 μL min^{-1}.

For all three microreactors, of the three channels near the fluidic ports, the largest fluid flow velocities were found in the middle channel. In this middle channel, a maximal fluid velocity of ≈6 mm s^{-1} in the centre of the channel was computed for a flow rate of 1000 μL min^{-1}. The outer channels returned a maximal velocity of ≈14 mm s^{-1}. These values were similar for all three microreactors. They are also like Macown et al. reported [25], who found the middle channel to exhibit the highest velocities.

The fluid velocity profile in the 'empty' reaction chamber was calculated as a mimic for the hydrogel microreactor, and at the same

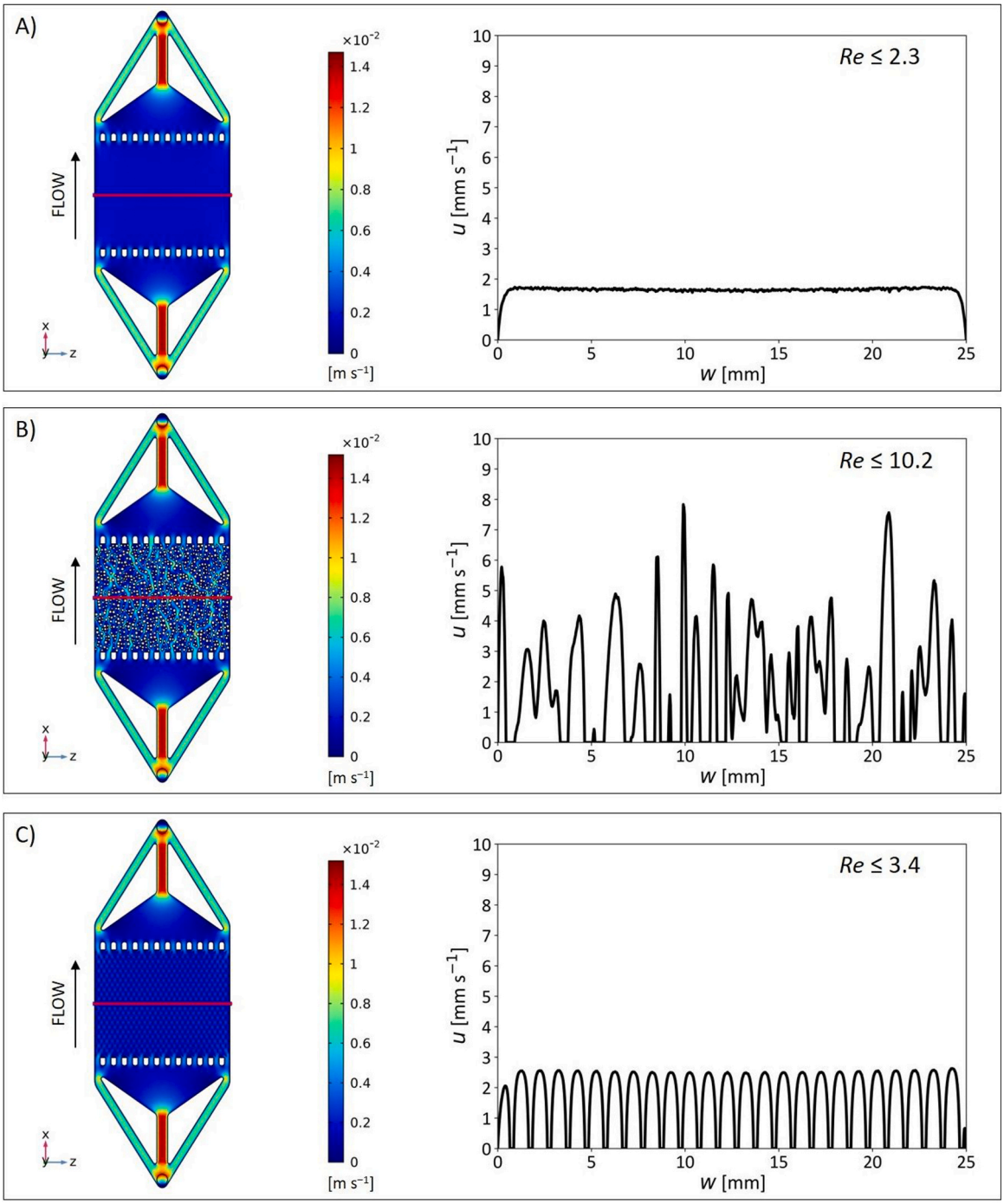

Fig. 4. Fluid flow characteristics in different microreactors when subjected to the maximum volumetric flow rate (Q_V = 1000 μL min^{-1}). **A)** The flow velocity distribution in an empty microreactor (mimicking the hydrogel microreactor). **B)** The flow velocity distribution when the reaction chamber is filled with randomly packed beads. **C)** The flow velocity distribution in the micropillar microreactor. The flow velocity profiles for each microreactor type (right-hand side plots) were calculated at half the depth ($d/2$) and half the length ($l/2$) of the reaction chamber throughout the entire width (w = 25 mm). The horizontal red line in each microreactor indicates the position where the velocity profiles were calculated.

time served as a benchmark for the other two reactor types. The velocity profile is depicted in Fig. 4A and shows a relatively uniform fluid flow distribution across the entire width of the reaction chamber (except for about ≈1 mm in the vicinity of the chamber walls). The maximal velocity of ≈ 1.7 mm s^{-1} (Fig. 4A) compares reasonably well with the imposed flow rate of 1000 μL min^{-1}. For the packed-bed microreactor with the beads randomly distributed the velocities varied between 0.5 mm s^{-1} and 7.8 mm s^{-1} (Fig. 4B). The velocity profile was expectedly not uniform, in line with the channelling typical of inconsistent bead packing. Such deviation from the plug flow profile negatively impacts biotransformation performance of packed bed reactor [14]. In contrast, the velocity profile for the micropillar microreactor has a regular pattern as can be seen in Fig. 4C. The maximal velocity magnitudes are ≈2.6 mm s^{-1}. For all reactor types, the Reynolds numbers were low, with the packed-bed reactor having the highest of about 10. These models were subsequently further validated using RTD analysis.

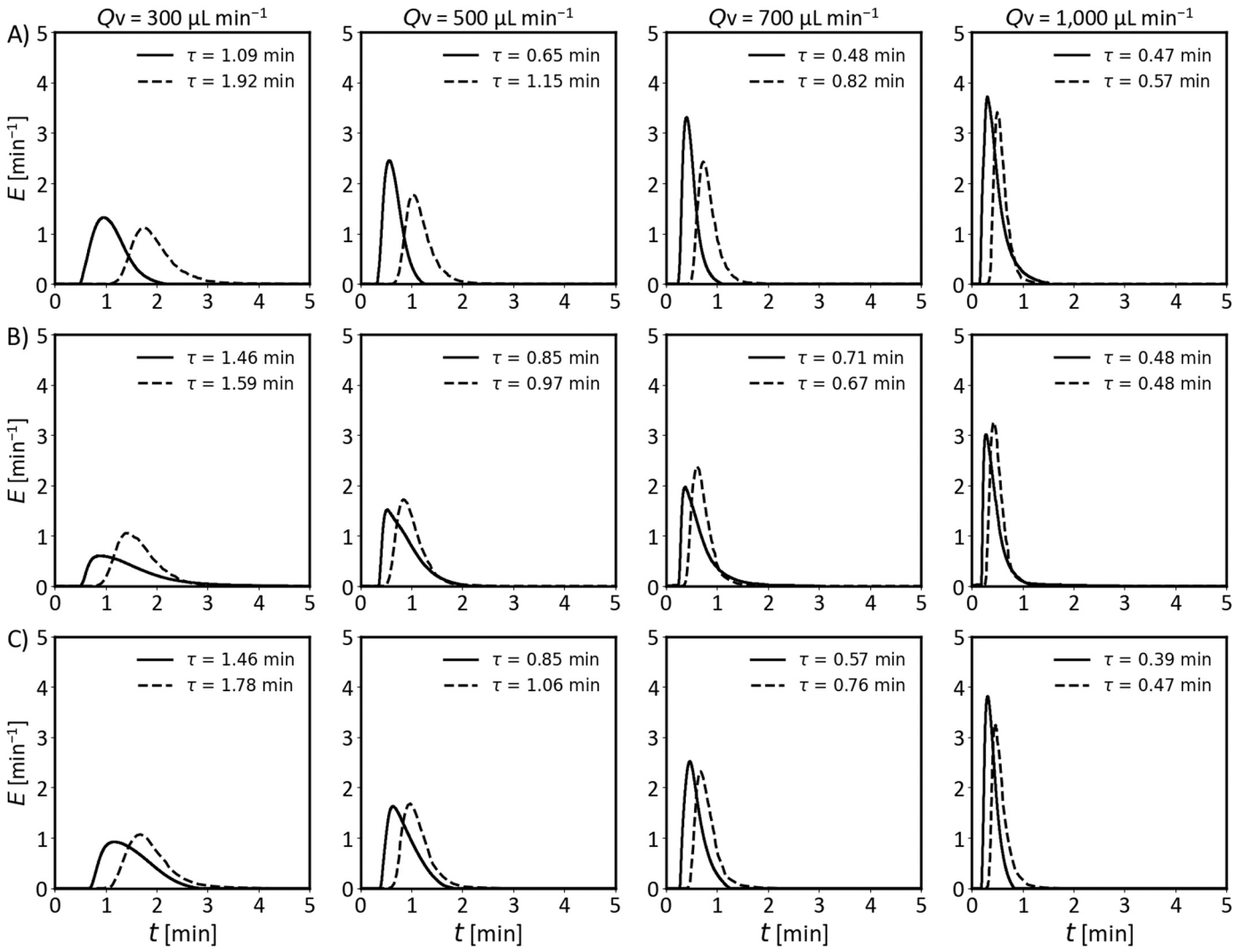

Fig. 5. *E* curves obtained from the RTD pulse experiment performed at various volumetric flow rates using 1 mM L-TRY as the inert tracer (the injection volume was ≈7.5 µL). **A)** Empty microreactor **B)** Packed-bed microreactor. **C)** Micropillar microreactor. **Legend:** (—) Experimental *E* curves, E_{exp}; (— –) Calculated *E* curves, E_{cal}.

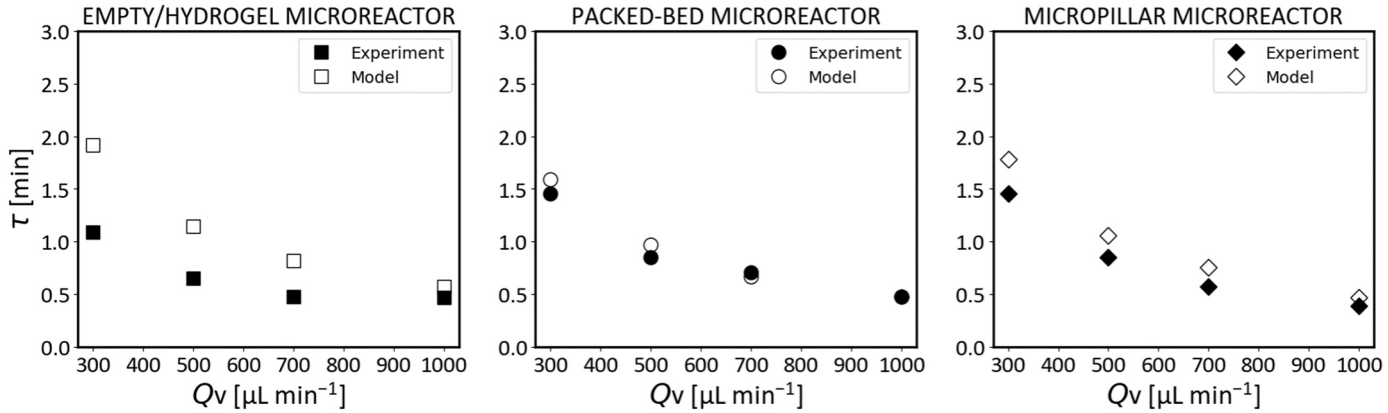

Fig. 6. Comparison between experimental and calculated mean residence times for each microreactor type. The mean residence times were calculated from the experimentally and theoretically established L -tryptophan concentration profiles, $c_{L\text{-}TRY}(t)$, at the outlet of the microreactors.

3.4. Residence Time Distribution analysis of the microreactor types

The CFD models established for the fluid velocity profiles were then expanded to mimic a tracer pulse experiment in the microreactors. For these models, we assumed an initial tracer concentration of 1 mM at the microreactor inlet port, convective transport in the axial direction of the flow, and diffusion in both radial and axial direction, and a concentration distribution at the microreactor outlet. The theoretical response curves at the outlet of all three microreactor types were established for the four flow rates, 300 µL min^{-1}, 500 µL min^{-1}, 700 µL min^{-1}, and

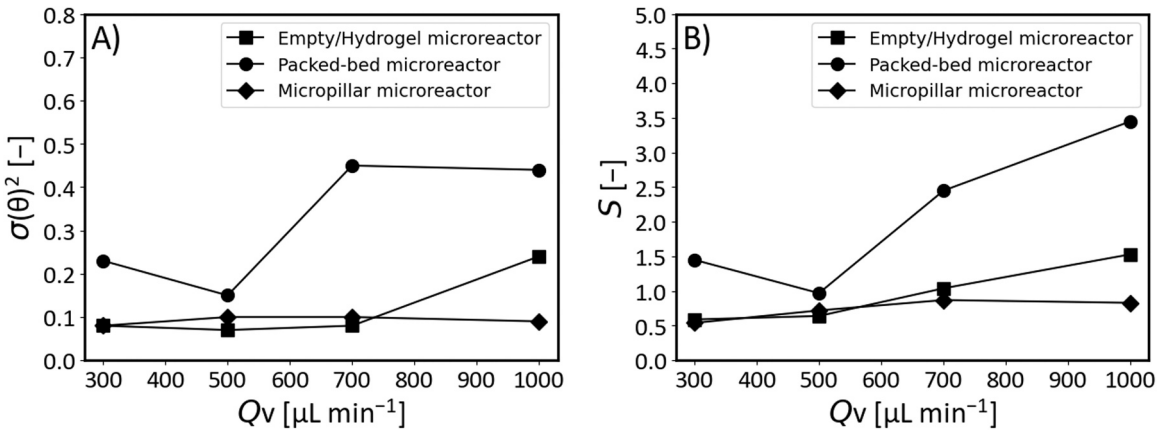

Fig. 7. The 2nd and 3rd moments of distribution. **A)** Variance (which is represented in its dimensionless form). **B)** Skewness. All values were calculated based on the experimental $c_{\text{L-TRY}}(t)$ distribution profiles.

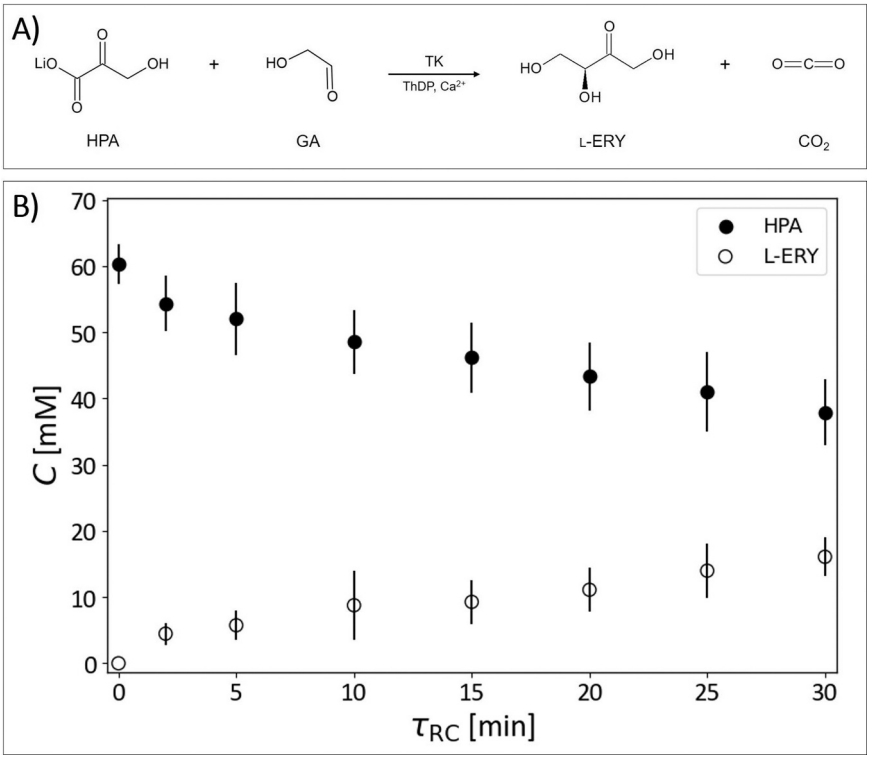

Fig. 8. A) TK-catalysed conversion of HPA and GA to L-ERY and CO_2 conducted in the presence of ThDP and Ca^{2+} ions. **B)** Reaction profiles in the hydrogel microreactor obtained under the following conditions: $c_{\text{HPA/GA}} = 60$ mM, $c_{\text{ThDP}} = 9.8$ mM, and $c_{\text{CaCl2}} = 2.4$ mM, all in HEPES buffer (50 mM; pH 7.0); $T = 20$ °C. **Abbreviations and acronyms:** TK, transketolase; HPA, lithium β-hydroxypyruvate; GA, glycolaldehyde; L-ERY, L-erythrulose; CO_2, carbon dioxide; ThDP, thiamine diphosphate.

1000 µL min^{-1}.

To validate the theoretical response curves, tracer pulse experiments were carried out using L-TRY, as the inert tracer. To minimise the dispersion of the tracer pulse due to the shear gradients in the tubing leading to and from the microreactor (Fig. 1), the length of tubing was kept to a minimum. The experimentally obtained E curves (E_{exp}) were compared with the E curves calculated using the established CFD models (E_{cal}). Fig. 5 shows the results for this comparison for three microreactors for flow rates between 300 µL min^{-1} to 1000 µL min^{-1}.

As can be seen from Fig. 5, all E curves (for all microreactors, and for both the model and the experimental data) showed a shift of their peak to shorter times and an increase in amplitude with increasing flow rates. This shift and the increase in amplitude match with the shorter residence time of the tracer in the reactors at higher flow rates. Also, for higher flow rates the model data is in good agreement with the experimental data. At lower flow rates, ≤500 µL min^{-1}, however, the deviation between the experimental and model curves becomes more prominent. To quantify this discrepancy, the mean residence times from experiment and model were compared for each reactor type, and a χ^2 test performed to determine goodness of fit between the two datasets (Fig. 6) [41].

The ${\chi_{cv}}^2$ for a 5% significance level ($\alpha = 0.05$) and for three degrees of freedom is 7.815. The obtained χ^2 values were 0.030, 0.009, and 0.002 for the empty, packed-bed and micropillar microreactors, respectively. Thus, the χ^2 values were smaller than ${\chi_{cv}}^2$ values for all microreactors, suggesting that the deviations observed are more likely to be the consequence of experimental variations than due to the existence

Table 2
Summary of the specifications and metrics in all microreactor types.

Microreactor type	Hydrogel	Packed-bed	Micropillar
Property / Reaction executed	*Transketolation*	*Transesterification*	*Transamination*
Void volume in the reaction chamber, V_V [μL]	298 ± 62[(a)]	175 ± 6[(a)]	268 ± 20[(a)]
Porosity of the reaction chamber, ε_{RC} [—]	N/A	0.58 ± 0.02[(b)]	0.89 ± 0.07[(b)]
Mean residence time in the reaction chamber, τ_{RC} [min]	2.0 — 30.0[(c)]	0.1 – 2.0[(c)]	2.0 – 45.0[(c)]
Biocatalyst concentration, c_B [$mg_{biocatalyst}$ mL_{void}^{-1}]	2.52 ± 0.11	38.77 ± 3.31	7.18 ± 0.31
Biocatalyst spec. activity, SA_B [U $mg_{biocatalyst}^{-1}$]	5.68 ± 0.01	110.14 ± 18.89[(d)]	0.79 ± 0.11
Biocatalyst load, Y_B [U mL_{void}^{-1}]	14.31 ± 0.64[(e)]	4270.1 ± 364.6[(e)]	5.67 ± 0.24[(e)]
Max. conversion, X [%]	37.41 ± 5.35	78.93 ± 5.38	3.17 ± 0.54
Max. volumetric productivity, Q_P [$mmol_{product}$ L_{void}^{-1} min^{-1}]	2.23 ± 0.83	317.69 ± 96.74	0.08 ± 0.02
Max. biocatalyst productivity number, *BPN* [$mmol_{product}$ $g_{biocatalyst}^{-1}$]	6.39 ± 1.15	4.25 ± 0.66	0.03 ± 0.01

[(a)]Calculated as the difference between the volume of the empty chamber and the carrier. The volume of N435 beads was calculated from their weighed mass and density (considered to be 0.555 mg μL^{-1}) [15].
[(b)]Calculated based on the reaction chamber, as the ratio between the reaction chamber void and total volume, $\varepsilon_{RC}=V_v/V$.
[(c)]Calculated based on the reaction chamber, as the ratio between the reaction chamber void volume and applied volumetric flow rate, $\tau_{RC}=V_v/Q_V$.
[(d)]Determined for the immobilised enzyme assuming that CaLB content was 10% w/w of N435 total mass [8,15].
[(e)]Calculated as the product between biocatalyst concentration and its specific activity, $Y_B = c_B \times SA_B$.

of stagnant zones. Additionally, the 2nd (variance) and 3rd (skewness) moments of the residence time distribution were compared for each microreactor type. The values of variance ranged from 0.07 to 0.45 (Fig. 7A), whereby the packed-bed microreactor exhibited slightly higher variance values compared to the other two microreactors. Similarly, the skewness (Fig. 7B), ranging between 0.54 and 3.45, is highest for the packed-bed microreactor, in line with the findings from the fluid flow velocity profiles calculated with. Overall, the comparison of the theoretical with the experimental *E* curves indicates that the fluid flow velocity profiles obtained are valid, and that therefore these profiles provide reasonable approximations of the hydrodynamic behaviour in the three microreactors.

3.5. Transketolase-catalysed biotransformations using whole cells in the hydrogel microreactor

The final test for our novel microreactor concept was to verify that biocatalytic reactions can be successfully executed. The first of these final tests was performed with the hydrogel microreactor. We entrapped *E. coli* cells overexpressing the enzyme TK into alginate hydrogel sheets, which had been attached to the bottom surface of the 'vertical' bar of the T-shaped lid. The TK-catalysed reaction synthesises L-erythrulose (L-ERY) from the non-chiral substrates hydroxypyruvate (HPA) and glycolaldehyde (GA), and L-ERY is a precursor for the synthesis of chiral amino alcohols (Fig. 8A) [37]. The reaction is fast, and CO_2 is produced as a by-product which allows achieving full conversion [7,37], making it thus a suitable choice to evaluate our novel microreactor.

The hydrogel sheet used had an average thickness of 591 ± 26 μm. Following its insertion into the microreactor by means of the T-shaped lid, a reaction chamber with a volume of about 300 μL was created. With the hydrogel sheets, we achieved a biocatalyst concentration of about 2.5 $mg_{biocatalyst}$ mL_{void}^{-1}. With a specific activity measured to be about 5.68 U $mg_{biocatalyst}^{-1}$, this meant a biocatalyst load of 14.31 U mL_{void}^{-1}. We set the flow rates to create mean residence times in the reaction chamber (τ_{RC}) between 2 min (Q_v = 149 μL min^{-1}) and 30 min (Q_v = 10 μL min^{-1}), and flowed a 60 mM equimolar solution of both non-chiral substrates through the microreactor (Fig. 8B). Under these conditions, a conversion of 37.41% was obtained at the highest residence time (τ_{RC} = 30 min). The corresponding maximal volumetric productivity and biocatalyst productivity number were 2.23 $mmol_{L\text{-}ERY}$ L_{void}^{-1} min^{-1} and 6.39 $mmol_{L\text{-}ERY}$ $g_{E.coli\ (DCW)}^{-1}$, respectively (Table 2). Previous studies have shown that similar conversion can be obtained in less than 5 min if free enzymes are used at an activity load of 3.25 U mL_{void}^{-1} [37]. The reduced efficiency can be attributed to mass transfer limitations through the alginate hydrogel matrix and across the cell membranes. To increase conversion, biocatalyst load could be increased, the gap between the hydrogel and the bottom of the chamber could be minimised, and the fluidisation degree of the hydrogel could be increased.

3.6. Lipase-catalysed biotransformations in the packed-bed microreactor

The packed-bed microreactor was evaluated using N435 beads, hydrophobic carriers made from an acrylic resin with the enzyme CaLB. This catalyst is widely used in the detergents, pharmaceuticals, biofuels, and food industry [42,43]. The reaction chosen used the enzyme CaLB to catalyse the conversion of vinyl butyrate (VB) and 1-butanol (1-BUT) into butyl butyrate (BB) and acetaldehyde (ACE) using *n*-heptane as a solvent (Fig. 9A). BB is a well-known pineapple-like fragrance [8].

The bed was packed using 67.9 mg of N435 beads (equivalent enzyme concentration of 38.77 mg_{CaLB} mL_{void}^{-1}) having an initial specific activity of 11.01 U mg_{N435}^{-1} (equivalent to 110.14 U mg_{CaLB}^{-1}). The resulting reaction chamber had a void volume of 175 μL with a porosity of ε_{RC} = 0.58, and a final resulting biocatalyst load of 4270.1 U mL_{void}^{-1}. This microreactor was tested with a 230 mM equimolar solution of both substrates pumped through the packed-bed at flow rates between 87 μL min^{-1} and 1750 μL min^{-1}. The maximum conversion obtained was 78.93% in 2 min (Fig. 9B), resulting in maximal volumetric productivity and biocatalyst productivity number of 317.69 $mmol_{BB}$ L_{void}^{-1} min^{-1} and 4.25 $mmol_{BB}$ g_{CaLB}^{-1}, respectively (Table 2). Complete conversion had been achieved previously with a similar reaction within 5 min at 25 °C using a catalyst concentration of ≈38.5 mg_{CaLB} mL_{void}^{-1} and a 500 mM substrate concentration in ionic liquids [8]. Lower conversions, closer in line with the ones of this study, achieved 79% conversion in roughly 0.2 min with 5530.0 U mL_{void}^{-1} resulting in a maximum biocatalyst productivity number of up to 14.03 $mmol_{BB}$ g_{CaLB}^{-1} [15]. Lower biocatalyst activity and reaction conditions (e.g., temperature) can account for the difference in yields.

3.7. Transaminase-catalysed biotransformations in the micropillar microreactor

The micropillars were incorporated directly in the T-shaped lid, arranged in a hexagonal pattern with diameter of 225 ± 11 μm, a height of 649 ± 17 μm and an interpillar distance of 437 ± 15 μm (Fig. S6, Appendix A). The micropillars were slightly longer than the chamber depth, which ensured that the pillars touched and compressed the PDMS bottom of the chamber. The wetted surface area was estimated to be 990 ± 75 mm^2. For this reactor, we chose the ω-TAm-catalysed conversion of (*S*)-(-)-α-methylbenzylamine ((*S*)-α-MBA) and sodium pyruvate (PYR) to acetophenone (ACP) and L-alanine (L-ALA) (Fig. 10A).

After insertion of the T-shaped lid, the estimated void volume of the reaction chamber was 268 μL, this with a porosity of ε_{RC} = 0.89. For this microreactor, the amount of protein which can be immobilised on the resin of the pillars was obtained from separately fabricated and larger

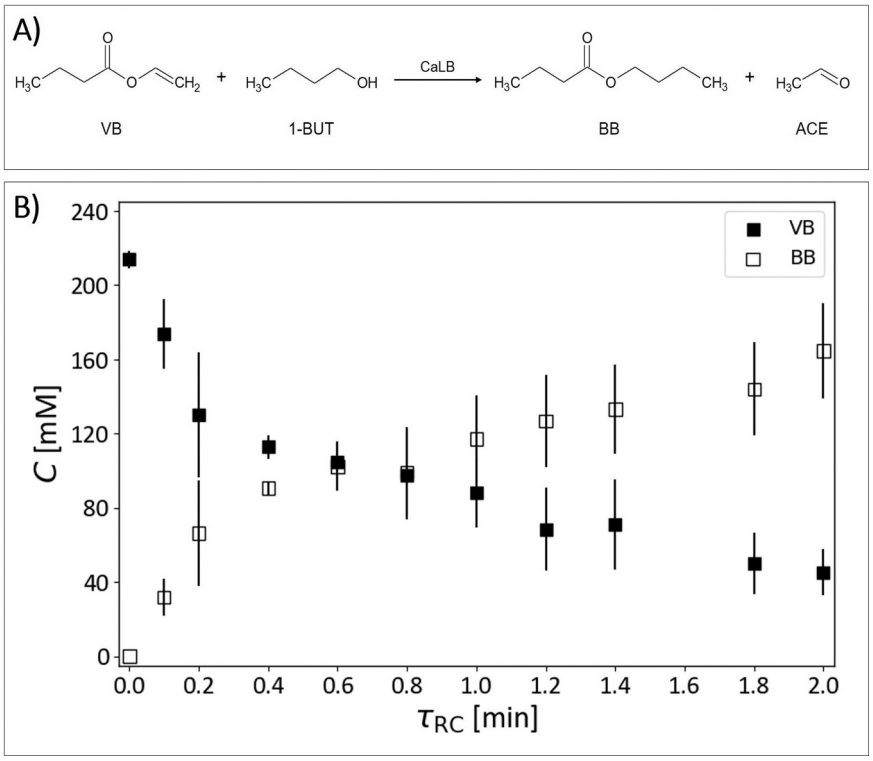

Fig. 9. A) CaLB-catalysed conversion of VB and 1-BUT to BB and ACE conducted in *n*-heptane. **B)** Reaction profiles in the packed-bed microreactor obtained under the following conditions: $c_{VB/1\text{-}BUT} = 230$ mM; $T = 20$ °C. **Abbreviations and acronyms:** CaLB, *Candida antarctica* lipase B; VB, vinyl butyrate; 1-BUT, 1-butanol; BB, butyl butyrate; ACE, acetaldehyde.

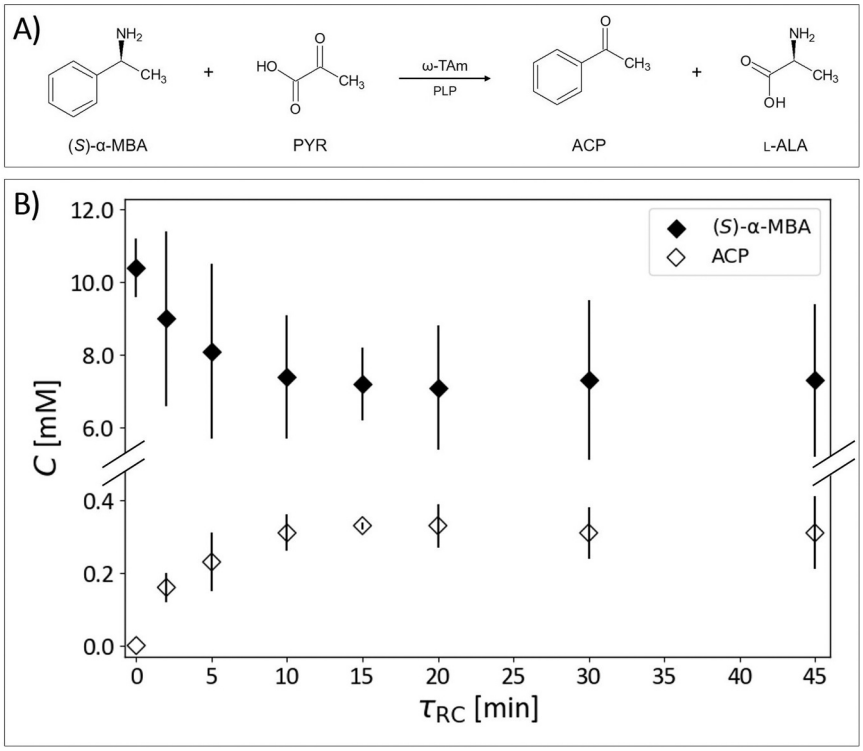

Fig. 10. A) ω-TAm-catalysed conversion of (*S*)-α-MBA and PYR to ACP and L-ALA conducted in the presence of PLP. **B)** Reaction profiles in the micropillar microreactor obtained under the following conditions: $C_{(S)\text{-}\alpha\text{-}MBA/PYR} = 10$ mM, $C_{PLP} = 1$ mM, all in HEPES buffer (50 mM; pH 7.5); $T = 20$ °C. **Abbreviations and acronyms:** ω-TAm, ω-transaminase; (*S*)-α-MBA; (*S*)-(-)-α-methylbenzylamine; PYR, sodium pyruvate; ACP, acetophenone; L-ALA, L-alanine; PLP, pyridoxal 5′-phosphate.

resin surfaces to minimise errors. We obtained an immobilisation efficiency of 1.94 ± 0.08 $\mu g_{protein}\ mm^{-2}_{surface}$, equivalent to a total of 1.92 ± 0.15 $mg_{protein}$ attached to the available surface area (Fig. S2, Appendix A). This resulted in a final concentration of 7.18 $mg_{protein}\ mL^{-1}_{void}$ and a biocatalyst load of 5.67 U mL^{-1}_{void} (Table 2). The microreactor was evaluated with 10 mM (*S*)-α-MBA and PYR and with flow rates between 6 μL min^{-1} and 134 μL min^{-1} (Fig. 10B). A conversion of 3.17% was attained at the mean residence time of τ_{RC} = 20 min (Fig. 10B). The maximum volumetric rate and biocatalyst productivity number were then 0.08 $mmol_{ACP}\ L^{-1}_{void}\ min^{-1}$ and 0.03 $mmol_{ACP}\ g^{-1}_{protein}$, respectively (Table 2). Transaminase-catalysed reactions are intrinsically slow [37]. To increase conversion, flow rates can be lowered to increase residence times, the biocatalyst load could be increased, and the micropillars could be positioned more closely to each other, enhancing the surface area to volume ratio for immobilisation.

4. Conclusions

The use of microreactors for process development has been hampered by a lack of standardised approaches which constrains industrial uptake. With immobilisation methods typically interlinked with the design of microreactors, performing a particular biocatalytic reaction may not only require finding an appropriate enzyme (as is often the case for biocatalytic process development in general), but may also require designing a new microreactor, or the re-design of an existing microreactor. In this contribution, we have shown for the first time that one microreactor design can be employed for different immobilisation methods and different biocatalytic applications. Furthermore, both whole-cell and enzyme based biotransformations have been carried out with the same microreactor design.

Based on a previously published design concept [22,23], we fabricated a microreactor which contained a T-shaped lid. The lid opens and closes the reaction chamber (without otherwise impacting the assembly of the microreactor), can easily be configured to accommodate different immobilisation methods, and facilitates straightforward insertion of biocatalysts, be they cells or enzymes. We successfully demonstrated introducing cells immobilised in hydrogels, enzymes immobilised in acrylic resin beads, and enzymes attached to a micropillar surface. These three immobilisation methods serve as examples to showcase the flexibility of the approach. The chamber is directly accessible and so is the bottom surface of the 'vertical' bar of our T-shaped lid in the 'open' configuration of the microreactor; it is thus probable that a wide range of other immobilisation supports, such as other polymeric matrices or monoliths, could be combined with this reactor design. Moreover, 3D-printing of the T-shaped lid offers a rapid turn-around from design to realisation of the lid; 3D-printing allows the rapid fabrication of different topographies at the bottom end of the 'vertical' bar' (as demonstrated with the micropillars). In the future, as more resins for 3D-printing are expected to become available, it will also facilitate other immobilisation chemistries.

To further illustrate the viability of this novel design, we performed biocatalytic reactions using the afore-mentioned immobilisation supports, effectively operating the device as three different reactor types: *E. coli* overexpressing TK was employed to perform a biotransformation in a hydrogel microreactor, resulting in the synthesis of L-erythrulose with a volumetric productivity of 2.23 ± 0.83 $mmol_{L\text{-}ERY}\ L^{-1}_{void}\ min^{-1}$; commercial beads with immobilised CaLB synthesised butyl butyrate, a well-known pineapple-like fragrance, in a packed-bed microreactor with a volumetric productivity of 317.69 ± 96.74 $mmol_{BB}\ L^{-1}_{void}\ min^{-1}$; the synthesis of acetophenone using a surface-immobilised ω-TAm-catalysed conversion in a micropillar microreactor with a volumetric productivity of 0.08 ± 0.02 $mmol_{ACP}\ L^{-1}_{void}\ min^{-1}$.

CFD models were created to analyse the fluid flow in these three microreactor types. For the 'empty' microreactor (mimicking the hydrogel microreactor), we obtained a velocity profile similar to a previously published design [22,25], whereas the packed-bed and micropillar microreactor type exhibited the channelling expected from random bead packing, and the regular patterns associated with a regular arrangement of the pillars, respectively. Using non-stationary models, CFD was applied to mimic a RTD experiment. The tracer pulse was both executed in an RTD experimental set-up and in the virtual CFD setting to further validate the CFD models. The similarity of the *E* curves obtained in theory and practice indicate that the CFD models are a valid representation of the flow behaviour in the three microreactors. Future work could include the combination of these models with enzyme kinetic models to improve our understanding of, and potentially also to predict the performance of biocatalytic reactions in the different microreactor types.

In summary, our contribution has introduced an innovative and versatile microreactor design which decouples design from the desired immobilisation method, and thus decouples microreactor design from application. Other groups and we have previously shown the cascading of microreactors and their in-line combination with separation and purification unit operations [6,10,37]. With this novel microreactor, the modularity of such cascades is significantly increased which will facilitate the realisation of factories-on-a-bench and underpin the faster development of biocatalytic processes. In addition to enhancing flexibility, the presented design also offers a step towards standardisation of microreactor technology. To perform different biotransformations, effectively only the T-shaped lid needs to be adapted. This adaptation may require the 3D-printing of a different lid design to change the topography of the bottom of end of the lid's 'vertical' bar, but it could also be as straightforward as simply exchanging a double-sided adhesive tape. All other parts would however remain the same, could therefore be standardised and made available to industry and academia as universal platform, thereby simplifying the supply logistics of parts. It is thus likely that the presented design will help pave the way towards off-the-shelf microreactor technology for biocatalysis.

CRediT authorship contribution statement

Marijan Bajić: Conceptualization, Methodology, Validation, Formal Analysis, Investigation, Writing - Original Draft, Writing - Review & Editing, Visualization. **Sansanee Khiawjan:** Methodology, Validation, Formal Analysis, Investigation. **Stephen T. Hilton:** Methodology, Resources. **Gary J. Lye:** Supervision, Project Administration, Funding Acquisition. **Marco P.C. Marques:** Conceptualization, Supervision, Funding Acquisition, Writing - Original Draft, Writing - Review & Editing. **Nicolas Szita:** Conceptualization, Supervision, Funding Acquisition, Writing - Original Draft, Writing - Review & Editing, Project Administration.

Declaration of Competing Interest

Patent applications derived from original GB Patent Application GB0821636.8 and PCT/GB2009/002778 A have been allowed or granted in the EU and the USA. N. Szita may become a potential beneficiary of these patents in the future.

Data Availability

Data will be made available on request.

Acknowledgements

This work received funding from the Future Biomanufacturing Research Hub (grant EP/S01778X/1), jointly supported by the Engineering and Physical Sciences Research Council (EPSRC) and the Biotechnology and Biological Sciences Research Council (BBSRC) as part of UK Research and Innovation (UKRI). The authors express their gratitude to Prof. John Ward of the UCL Department of Biochemical Engineering for generously providing *E. coli* strains from his cell bank.

Appendix A. Supporting information

Supplementary data associated with this article can be found in the online version at doi:10.1016/j.bej.2024.109260.

References

[1] A.I. Benítez-Mateos, M.L. Contente, D. Roura Padrosa, F. Paradisi, Flow biocatalysis 101: design, development and applications, React. Chem. Eng. 6 (2021) 599–611, https://doi.org/10.1039/d0re00483a.

[2] P. De Santis, L.E. Meyer, S. Kara, The rise of continuous flow biocatalysis-fundamentals, very recent developments and future perspectives, React. Chem. Eng. 5 (2020) 2155–2184, https://doi.org/10.1039/d0re00335b.

[3] L. Tamborini, P. Fernandes, F. Paradisi, F. Molinari, Flow bioreactors as complementary tools for biocatalytic process intensification, Trends Biotechnol. 36 (2018) 73–88, https://doi.org/10.1016/j.tibtech.2017.09.005.

[4] P. Žnidaršič-Plazl, Let the biocatalyst flow, Acta Chim. Slov. 68 (2021) 1–16, https://doi.org/10.17344/acsi.2020.6488.

[5] P. Gruber, M.P.C. Marques, B. O'Sullivan, F. Baganz, R. Wohlgemuth, N. Szita, Conscious coupling: the challenges and opportunities of cascading enzymatic microreactors, Biotechnol. J. 12 (2017) 1–13, https://doi.org/10.1002/biot.201700030.

[6] P. Fernandes, C.C.C.R. de Carvalho, Multi-enzyme systems in flow chemistry, Processes 9 (2021) 1–23, https://doi.org/10.3390/pr9020225.

[7] J. Lawrence, B. O'Sullivan, G.J. Lye, R. Wohlgemuth, N. Szita, Microfluidic multi-input reactor for biocatalytic synthesis using transketolase, J. Mol. Catal. B Enzym. 95 (2013) 111–117, https://doi.org/10.1016/j.molcatb.2013.05.016.

[8] A. Pohar, P. Žnidaršič-Plazl, I. Plazl, Integrated system of a microbioreactor and a miniaturized continuous separator for enzyme catalyzed reactions, Chem. Eng. J. 189–190 (2012) 376–382, https://doi.org/10.1016/j.cej.2012.02.035.

[9] C. Hu, Z. Huang, M. Jiang, Y. Tao, Z. Li, X. Wu, D. Cheng, F. Chen, Continuous-flow asymmetric synthesis of (3*R*)-3-hydroxyl-5-hexenoates with co-immobilized ketoreductase and *Lactobacillus kefir* dehydrogenase integrating greener inline microfluidic liquid-liquid extractors and membrane separators, ACS Sustain. Chem. Eng. 9 (2021) 8990–9000, https://doi.org/10.1021/acssuschemeng.1c01419.

[10] B. O'Sullivan, H. Al-Bahrani, J. Lawrence, M. Campos, A. Cázares, F. Baganz, R. Wohlgemuth, H.C. Hailes, N. Szita, Modular microfluidic reactor and inline filtration system for the biocatalytic synthesis of chiral metabolites, J. Mol. Catal. B Enzym. 77 (2012) 1–8, https://doi.org/10.1016/j.molcatb.2011.12.010.

[11] P. Gruber, M.P.C. Marques, N. Szita, T. Mayr, Integration and application of optical chemical sensors in microbioreactors, Lab Chip 17 (2017) 2693–2712, https://doi.org/10.1039/c7lc00538e.

[12] P. Gruber, M.P.C. Marques, P. Sulzer, R. Wohlgemuth, T. Mayr, F. Baganz, N. Szita, Real-time pH monitoring of industrially relevant enzymatic reactions in a microfluidic side-entry reactor (μSER) shows potential for pH control, Biotechnol. J. 12 (2017) 1–13, https://doi.org/10.1002/biot.201600475.

[13] J.M. Bolivar, F. López-Gallego, Characterization and evaluation of immobilized enzymes for applications in flow reactors, Curr. Opin. Green. Sustain. Chem. 25 (2020) 100349, https://doi.org/10.1016/j.cogsc.2020.04.010.

[14] M. Bajić, I. Plazl, R. Stloukal, P. Žnidaršič-Plazl, Development of a miniaturized packed bed reactor with ω-transaminase immobilized in LentiKats®, Process Biochem 52 (2017) 63–72, https://doi.org/10.1016/j.procbio.2016.09.021.

[15] F. Strniša, M. Bajić, P. Panjan, I. Plazl, A.M. Sesay, P. Žnidaršič-Plazl, Characterization of an enzymatic packed-bed microreactor: Experiments and modeling, Chem. Eng. J. 350 (2018) 541–550, https://doi.org/10.1016/j.cej.2018.05.028.

[16] T. Peschke, M. Skoupi, T. Burgahn, S. Gallus, I. Ahmed, K.S. Rabe, C.M. Niemeyer, Self-immobilizing fusion enzymes for compartmentalized biocatalysis, ACS Catal. 7 (2017) 7866–7872, https://doi.org/10.1021/acscatal.7b02230.

[17] G. Kulsharova, N. Dimov, M.P.C. Marques, N. Szita, F. Baganz, Simplified immobilisation method for histidine-tagged enzymes in poly(methyl methacrylate) microfluidic devices, N. Biotechnol. 47 (2018) 31–38, https://doi.org/10.1016/j.nbt.2017.12.004.

[18] N. Miložič, M. Lubej, M. Lakner, P. Žnidaršič-Plazl, I. Plazl, Theoretical and experimental study of enzyme kinetics in a microreactor system with surface-immobilized biocatalyst, Chem. Eng. J. 313 (2017) 374–381, https://doi.org/10.1016/j.cej.2016.12.030.

[19] D. Valikhani, J.M. Bolivar, M. Viefhues, D.N. McIlroy, E.X. Vrouwe, B. Nidetzky, A spring in performance: Silica nanosprings boost enzyme immobilization in microfluidic channels, ACS Appl. Mater. Interfaces 9 (2017) 34641–34649, https://doi.org/10.1021/acsami.7b09875.

[20] E. Gkantzou, K. Govatsi, A.V. Chatzikonstantinou, S.N. Yannopoulos, H. Stamatis, Development of a ZnO nanowire continuous flow microreactor with *β*-glucosidase activity: characterization and application for the glycosylation of natural products, ACS Sustain. Chem. Eng. 9 (2021) 7658–7667, https://doi.org/10.1021/acssuschemeng.1c02557.

[21] T. Menegatti, P. Žnidaršič-Plazl, Hydrogel-based enzyme and cofactor co-immobilization for efficient continuous transamination in a microbioreactor, Front. Bioeng. Biotechnol. 9 (2021) 1–10, https://doi.org/10.3389/fbioe.2021.752064.

[22] M. Reichen, R.J. Macown, N. Jaccard, A. Super, L. Ruban, L.D. Griffin, F. S. Veraitch, N. Szita, Microfabricated modular scale-down device for regenerative medicine process development, PLoS One 7 (2012), https://doi.org/10.1371/journal.pone.0052246.

[23] M. Reichen, A. Super, M.J. Davies, R.J. Macown, B. O'Sullivan, T.V. Kirk, M.P. C. Marques, N. Dimov, N. Szita, Characterisation of an adhesive-free packaging system for polymeric microfluidic biochemical devices and reactors, Chem. Biochem. Eng. Q. J. 28 (2014) 189–202, https://doi.org/10.15255/CABEQ.2014.1937.

[24] M. Reichen, F.S. Veraitch, N. Szita, Development of a multiplexed microfluidic platform for the automated cultivation of embryonic stem cells, J. Lab. Autom. 18 (2013) 519–529, https://doi.org/10.1177/2211068213499917.

[25] R.J. Macown, F.S. Veraitch, N. Szita, Robust, microfabricated culture devices with improved control over the soluble microenvironment for the culture of embryonic stem cells, Biotechnol. J. 9 (2014) 805–813, https://doi.org/10.1002/biot.201300245.

[26] N. Abdolvand, R. Tostoes, W. Raimes, V. Kumar, N. Szita, F. Veraitch, Long-term retinal differentiation of human induced pluripotent stem cells in a continuously perfused microfluidic culture device, Biotechnol. J. 14 (2019), https://doi.org/10.1002/biot.201800323.

[27] N. Jaccard, R.J. Macown, A. Super, L.D. Griffin, F.S. Veraitch, N. Szita, Automated and online characterization of adherent cell culture growth in a microfabricated bioreactor, J. Lab. Autom. 19 (2014) 437–443, https://doi.org/10.1177/2211068214529288.

[28] A. Super, N. Jaccard, M.P.Cardoso Marques, R.J. Macown, L.D. Griffin, F. S. Veraitch, N. Szita, Real-time monitoring of specific oxygen uptake rates of embryonic stem cells in a microfluidic cell culture device, Biotechnol. J. 11 (2016) 1179–1189, https://doi.org/10.1002/biot.201500479.

[29] W. Raimes, M. Rubi, A. Super, M.P.C. Marques, F. Veraitch, N. Szita, Transfection in perfused microfluidic cell culture devices: a case study, Process Biochem 59 (2017) 297–302, https://doi.org/10.1016/j.procbio.2016.09.006.

[30] N. Zhang, P. Domínguez de María, S. Kara, Biocatalysis for the synthesis of active pharmaceutical ingredients in deep eutectic solvents: state-of-the-art and prospects, Catalysts 14 (2024) 84, https://doi.org/10.3390/catal14010084.

[31] J.P. Adams, M.J.B. Brown, A. Diaz-Rodriguez, R.C. Lloyd, G.D. Roiban, Biocatalysis: A pharma perspective, Adv. Synth. Catal. 361 (2019) 2421–2432, https://doi.org/10.1002/adsc.201900424.

[32] S. Wu, R. Snajdrova, J.C. Moore, K. Baldenius, U.T. Bornscheuer, Biocatalysis: Enzymatic synthesis for industrial applications, Angew. Chem. - Int. Ed. 60 (2021) 88–119, https://doi.org/10.1002/anie.202006648.

[33] L. Panariello, L. Mazzei, A. Gavriilidis, Modelling the synthesis of nanoparticles in continuous microreactors: The role of diffusion and residence time distribution on nanoparticle characteristics, Chem. Eng. J. 350 (2018) 1144–1154, https://doi.org/10.1016/j.cej.2018.03.167.

[34] A. Cantu-Perez, S. Bi, S. Barrass, M. Wood, A. Gavriilidis, Residence time distribution studies in microstructured plate reactors, Appl. Therm. Eng. 31 (2011) 634–639, https://doi.org/10.1016/j.applthermaleng.2010.04.024.

[35] A. Cantu-Perez, S. Barrass, A. Gavriilidis, Residence time distributions in microchannels: comparison between channels with herringbone structures and a rectangular channel, Chem. Eng. J. 160 (2010) 834–844, https://doi.org/10.1016/j.cej.2009.07.023.

[36] C.R. Wilke, P. Chang, Correlation of diffusion coefficients in dilute solutions, AIChE J. 1 (1955) 264–270, https://doi.org/10.1002/aic.690010222.

[37] P. Gruber, F. Carvalho, M.P.C. Marques, B. O'Sullivan, F. Subrizi, D. Dobrijevic, J. Ward, H.C. Hailes, P. Fernandes, R. Wohlgemuth, F. Baganz, N. Szita, Enzymatic synthesis of chiral amino-alcohols by coupling transketolase and transaminase-catalyzed reactions in a cascading continuous-flow microreactor system, Biotechnol. Bioeng. 115 (2018) 586–596, https://doi.org/10.1002/bit.26470.

[38] S.R.A. Kratz, C. Eilenberger, P. Schuller, B. Bachmann, S. Spitz, P. Ertl, M. Rothbauer, Characterization of four functional biocompatible pressure-sensitive adhesives for rapid prototyping of cell-based lab-on-a-chip and organ-on-a-chip systems, Sci. Rep. 9 (2019) 1–12, https://doi.org/10.1038/s41598-019-45633-x.

[39] M.M. Bradford, A rapid and sensitive method for the quantitation of microgram quantities of protein utilizing the principle of protein-dye binding, Anal. Biochem. 72 (1976) 248–254, https://doi.org/10.1016/0003-2697(76)90527-3.

[40] A.S. Bommarius, M.F. Paye, Stabilizing biocatalysts, Chem. Soc. Rev. 42 (2013) 6534–6565, https://doi.org/10.1039/c3cs60137d.

[41] N.A. Sayar, B.H. Chen, G.J. Lye, J.M. Woodley, Modelling and simulation of a transketolase mediated reaction: sensitivity analysis of kinetic parameters, Biochem. Eng. J. 47 (2009) 1–9, https://doi.org/10.1016/j.bej.2009.02.011.

[42] C. Ortiz, M.L. Ferreira, O. Barbosa, J.C.S. Dos Santos, R.C. Rodrigues, Á. Berenguer-Murcia, L.E. Briand, R. Fernandez-Lafuente, Novozym 435: the "perfect" lipase immobilized biocatalyst? Catal. Sci. Technol. 9 (2019) 2380–2420, https://doi.org/10.1039/c9cy00415g.

[43] H. hai Wang, Q. Zhang, X. Yu, J. Liang, Y. Zhang, Y. Jiang, W. Su, Application of lipase B from *Candida antarctica* in the pharmaceutical industry, Ind. Eng. Chem. Res. 62 (2023) 15733–15751, https://doi.org/10.1021/acs.iecr.3c02132.